FLOW INSTABILITY IN AN ALUMINA PRECIPITATOR FITTED WITH A DRAFT TUBE CIRCULATOR

Graeme LANE[1]

[1] CSIRO Minerals, Box 312, Clayton Sth, Victoria 3169, AUSTRALIA

ABSTRACT

In this study, the fluid flow in alumina precipitators with draft tube circulators has been investigated. These precipitators are operated with a quiescent zone at the surface whereby settling of solids achieves partial clarification of the overflow stream. However, plant operating experience has shown that there is a difference in solids concentration at the overflow depending on the tank design. To investigate the reasons for this variation, CFD modelling has been carried out for tanks of the same diameter but differing aspect ratios. Initially, steady-state simulations were carried out, which indicated the presence of a recirculating vortex in the lower part of the annulus. Turbulence intensity in the vicinity of this vortex, as predicted from the k-epsilon model, was high, suggesting that the flow pattern might in fact be unsteady. Therefore, for further insight, transient large eddy simulations were carried out. These showed similar flow structures but a flow pattern with large time variations. It is thought that intermittent surges from the recirculating vortex can transport solids into the clarifying layer. Since the vortex is closer to the surface in the shorter tank, average solids concentration reporting to the overflow launder is higher.

NOMENCLATURE

C_S Smagorinsky constant (-)
I turbulence intensity (-)
$\mathbf{S}$ rate of strain tensor (1/s)
V_{cell} cell volume(m^3)
u_0 fluctuating velocity (m/s)
$\mathbf{U}$ mean velocity (m/s)
ν kinematic eddy viscosity (m^2/s)
τ shear stress (Pa)

INTRODUCTION

A computational fluid dynamics (CFD) modelling study has been carried out to investigate the slurry flow in alumina precipitator tanks. These tanks form part of a plant employing the Bayer process for production of alumina from bauxite. Mixing in these tanks is achieved using draft tube circulators, where a downward-pumping axial flow impeller is located inside a draft tube. In this study, the flow behaviour has been investigated and compared for two different tank designs.

Draft tubes are employed in mechanically-stirred tanks for a number of applications, particularly for crystallisations, where a high degree of homogeneity is required, and also for operations such as mixing of viscous materials. The use of a draft tube provides for effective top-to-bottom circulation (Paul et al., 2004). The application of draft tube circulators for alumina hydrate precipitation has been described by Shaw (1982). For economic production, these tanks are very large with a high aspect ratio, typically 10 to 12 metres in diameter and up to 40 metres high. Draft tube circulators have become favoured for this application because it is critical at this large scale to minimise the energy input for mixing, and this design offers energy-saving benefits compared to earlier installations, which have employed air lifts (Pachuca tanks) or mechanical agitation by multiple impellers.

In the tanks considered here, although the aim is to achieve uniform mixing over most of the tank, the tanks have also been designed to provide a quiescent zone above the level of the draft tube. It is intended that solids will settle in this zone, so that a degree of clarification of the overflow stream from each tank can be achieved. The particular focus in this study was to investigate how differences in the solids concentration at the overflow are related to variations in the tank design. More specifically, two tanks were modelled which both had the same draft tube diameter and the same overall diameter, but differed in their liquid heights, i.e. in the tank aspect ratio. They are agitated by the same impeller type at the same speed. Operating experience has indicated that the degree of clarification of the overflow is higher for the taller tank, but the reasons for this have not been fully understood. By studying the internal slurry flow in detail, this study aimed to provide better understanding of the flow pattern in each tank, so as to discern how differences in flow pattern affect the extent of clarification at the overflow.

Several studies have been reported in the literature where stirred tanks with draft tubes have been investigated. For example, Aeschbach and Bourne (1972) carried out an experimental study in which they developed an optimised tank geometry with a draft tube and a profiled base, so as to achieve homogeneous suspension of solids in a continuous flow crystalliser. Aubin et al. (2000) carried out CFD modelling of a tank agitated by a helical screw impeller. The CFD model was applied to laminar flow of Newtonian and shear thinning liquids, and flow patterns and mixing time were compared for tanks with and without a draft tube. Kumaresan et al. (2005) carried out a study of the turbulent fluid flow in a laboratory-scale tank equipped with a hydrofoil impeller and a draft tube, in which they made measurements of velocities and power consumption for draft tubes of two alternative lengths. In addition, they developed a CFD model based on the Reynolds-averaged equations for mass and momentum conservation, in conjunction with the k-epsilon turbulence

model. The CFD model was found to give good predictions of velocities, power and mixing time.

Previous studies such as these have not addressed the issue concerning these particular alumina precipitators, namely the requirement for clarification at the surface. Also, previous CFD studies of turbulent flow in tanks with draft tubes have been based on the Reynolds-averaged equations. This approach was also adopted here, but in addition, the large eddy simulation (LES) method has been implemented. LES was introduced since it was suspected that the flow is inherently unsteady, and this method is more suitable for characterising the time-dependent flow. Large eddy simulation has been previously applied to model stirred tanks with open impeller types (e.g. Eggels, 1996; Hartmann et al., 2004), but it does not appear to have been previously applied to tanks with draft tubes.

DETAILS OF THE TANKS

In the two tank designs considered here, both tanks have an external diameter of 14 m and a draft tube diameter of 4.6 m, but the tanks differ in the overall liquid height and draft tube height, the shorter tank having a liquid height of 27.5 m and a draft tube height of 19 m, and the taller tank having a liquid height of 36 m and a draft tube height of 27 m. The tanks follow a design similar to that recommended by Shaw (1982), with a downward pumping agitator (Lightnin C110 type) located inside the draft tube towards the top of the draft tube. The draft tube is fitted with flow-straightening vanes and is slotted, so that in the case of a shut-down, the bottom of the draft tube is not blocked off by settling solids, but instead the liquid can flow through the slots, gradually eroding the settled bed of solids. The tanks have a flat bottom with a filleted corner and centre to avoid solids build-up. Slurry is fed to the tank through a pipe extending towards the bottom, and slurry is removed in two streams, an underflow pipe and an overflow launder. The agitator speed and inlet and outlet flow rates were the same for each tank, and the average solids concentration was assumed to be the same.

MODELLING METHOD

Steady-state Simulations

For the steady-state simulations in the initial stage of the study, block-structured body-fitted finite volume meshes were generated using the program CFX Meshbuild, to represent the geometry of the precipitator tanks. The meshes are illustrated in Figure 1. The draft tube was represented by a 'thin surface', ignoring the actual wall thickness. To reduce the complexity of the problem, the impeller was not explicitly represented, since it was expected that, being located inside a draft tube with flow-straightening vanes, the impeller would produce a fairly uniform downward flow. Therefore, a uniform momentum source term was imposed at the position of the impeller to represent the flow induced by the impeller, with the velocity set to give a circulation flow of 67 000 m^3/hr. The finite volume mesh for each tank consisted of about 230 000 cells.

Based on these finite volume meshes, the steady-state equations for conservation of mass and momentum were solved using the CFX4 code. Since the flow is turbulent, the equations were solved in the Reynolds-averaged form, for which closure was obtained with the standard k-epsilon turbulence model. At all walls, a no-slip condition was applied, and wall functions were applied to account for the steep, unresolved velocity profile in the boundary layers. The surface was taken to be flat with a free-slip boundary condition.

The distribution of suspended solids was accounted for by using the Algebraic Slip Model. In this approach, the solids are represented by a number of size classes, and the flow field for each class of particles is obtained by the vector addition of the background liquid phase velocity and the particle terminal settling velocity. Based on this flow field and an initial guess for the distribution of the particles, the local concentration of particles in each size class is calculated at each iteration. Then, based on the local mass fractions of each solids class and the background liquid phase, a spatially-varying density is calculated. For the purposes of the calculation, the particle size distribution as measured at the plant was represented by four size classes, with mean sizes of 20, 55, 85, and 145 μm.

The equations were solved using a hybrid central/upwind differencing scheme for the convective terms and a second order accurate scheme for all other terms. Convergence of the solution was judged based on sufficient reduction of the overall residual error for each equation and a flow field which did not change with further iterations. About 2500 iterations were required.

Large Eddy Simulations

Results of the steady-state simulations suggested that the flow may in fact be inherently unsteady. Therefore, for further understanding of the flow behaviour, additional simulations were carried out to model the time-dependent flow in the tanks. Here, the large eddy simulation (LES) approach was implemented. In this method, the larger turbulent eddies, with length scales greater than the grid spacing, are modelled explicitly, while the smaller scales of turbulence remain unresolved, but are accounted for by modelling the sub-grid stress using a relatively simple turbulence model, based on an assumption of the universal, isotropic nature of turbulence at small scales.

The LES approach is based on a spatially filtered form of the conservation equations, where the filter is similar in size to the mesh spacing. For closure of the equations, the sub-grid stress has been assumed to follow the eddy viscosity hypothesis. Hence, the sub-grid stress, τ, is assumed to be given by:

$$\tau = -2v_{SGS}\overline{\mathbf{S}} , \qquad (1)$$

where $\overline{\mathbf{S}}$ is the strain rate tensor of the filtered large scale flow, and v_{SGS} is the eddy viscosity. Following the Smagorinsky model, the viscosity is taken to be dependent on the gradients of the filtered velocity and a length scale related to the grid size, and is therefore given as:
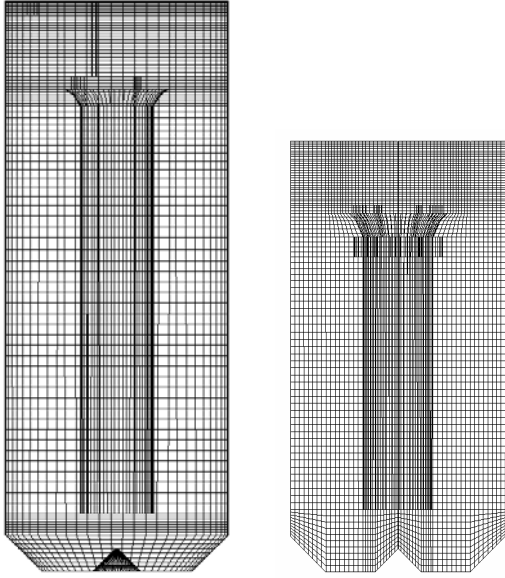
Figure 1: Block-structured finite volume meshes plotted on surfaces for taller and shorter tanks, as used in steady-state model.

$$v_{SGS} = \left(C_s V_{cell}^{1/3} \right)^2 \left| \overline{\mathbf{S}} \right|, \tag{2}$$

where V_{cell} is the cell volume, $\left| \overline{\mathbf{S}} \right|$ is the modulus of the strain rate tensor, and the Smagorinsky constant, C_S, was taken as 0.1.

Simulations were carried out using the CFX5 code. This change in CFD code was necessary in order to obtain a mesh with fairly uniform cell volumes. With LES, it appeared to be important to make cell volumes as uniform as possible, since large variations in cell volume lead to different filtering length scales in different parts of the flow domain, which may lead to a bias in the predicted flow. With a cylindrical-type geometry using a structured mesh, as was used with CFX4, uniform cell sizes were not possible. However, a uniform mesh can be obtained with an unstructured mesh. To model the fluid flow with such a mesh, it was necessary to change to CFX5. Hence, new finite volume meshes were generated using unstructured, tetrahedral elements. However, although cell volumes were made uniform over most of the tank, it was also found to be important to resolve eddies in the boundary layer, so the grid at the walls was made considerably finer, using prismatic cells for "inflation" layers.

In principle, the full geometry should have been included in the flow domain, since strictly speaking there are no planes of symmetry or periodicity when the turbulent flow structures are resolved. However, to reduce the computational demand, only one quarter of the tanks were modelled with periodic boundaries in the azimuthal direction. This can be justified since the mean flow field is quite uniform circumferentially, and a 90 degree section would extend over several integral length scales of the turbulence. A further simplification to reduce the total grid size was that the region inside the draft tube was omitted from the solution domain. This was justified since interest was in the flow in the outer and top parts of

the tank. An inlet was set at the bottom of the draft tube and a mass flow boundary was set at the top of the draft tube, with the mean velocity at the inlet set to give the correct circulation flow. The unstructured meshes are illustrated in Figure 2. The total number of elements was about 420 000 for the shorter tank and 630 000 for the taller tank.

A steady-state solution was first obtained using a method similar to that described earlier, and this was used as an initial guess for the LES. Time steps of 0.5 seconds were used, with 4 iterations per time step. A total of ~10 minutes of real time was calculated for each tank. However, it was estimated that it took about 5.5 minutes to achieve fully-developed flow. Therefore, average values of parameters extracted from the LES were based only on the last 4.5 minutes (real time) of simulation.

RESULTS

Steady-state simulations

The flow patterns obtained from the steady-state simulations are illustrated by the vector plots in Figure 3. These plots are for velocity vectors in one vertical slice passing through the centre of the taller tank, but the flow pattern is essentially axisymmetric, except for the flow near the top of the tank which is influenced by the overflow launder. The flow pattern is not quite as has been generally conceptualised for a tank with a draft tube, since it is usually assumed (e.g. Shaw, 1982) that the flow circulates from top to bottom in a single loop, with
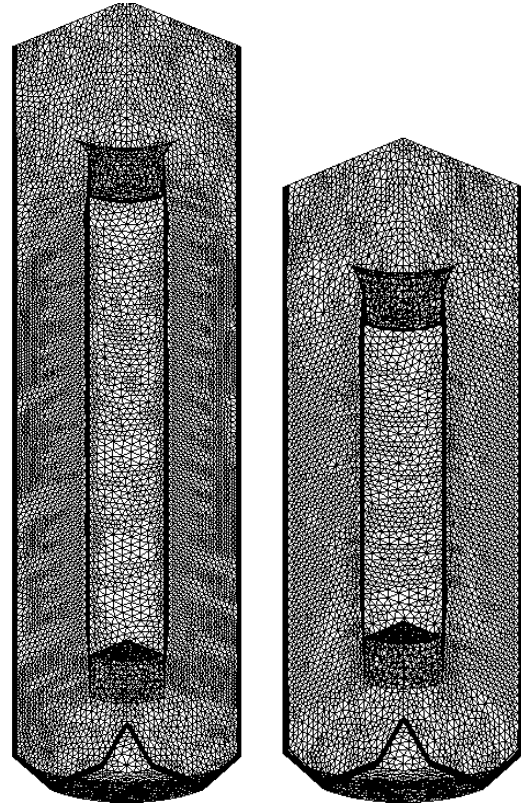

Figure 2: Unstructured tetrahedral grids with prismatic inflation layers, as used for large eddy simulations.

unidirectional axial flow in the draft tube and the annulus. Instead, there is recirculation within the annulus. Such a recirculation was noted by Aeschbach and Bourne (1972) in their laboratory tank, although they did not take detailed measurements. The CFD results here indicate that there is flow separation from the draft tube wall as the discharge flow from the bottom of the draft tube turns through 180 degrees, and this results in reversal of flow back down along the outer side of the draft tube, i.e. a large recirculation loop is formed in the lower part of the annulus. Further up the annulus, the high velocity flow near the outer wall spreads out, and the flow reattaches to the draft tube wall.

When the two tanks are compared side by side, the overall flow pattern and magnitude of velocities are very similar. A point of significance is that the recirculation loop has the same height in each tank, even though the draft tube and the tank vary in height. Therefore, the recirculation loop extends considerably closer to the surface of the shorter tank.

In Figure 4, the turbulence intensity, *I*, is plotted, as defined by:

$$I = \frac{u_0}{|\mathbf{U}|} \,, \tag{3}$$

where u_0 is the r.m.s. fluctuating velocity (obtained from the turbulent kinetic energy) and $\mathbf{U}$ is the mean velocity. This parameter can give a measure of how stable the flow is in different regions. For comparison, fully-developed turbulent flow in pipes would be expected to have a turbulence intensity of about 0.05 – 0.1. Here, turbulence intensities greater than 1 are found in association with the recirculation loop, and also near the surface. For the recirculation loop, this means that the flow would be expected to be highly unstable, since the fluctuating velocities can be greater than the mean velocity. Therefore, the instantaneous flow pattern in the annulus could vary considerably.

Since the physical dimensions of the recirculating vortex are about the same for both tanks, the vortex in the shorter tank extends considerably closer to the top of the tank, and hence instabilities in the flow would have greater proximity to the surface.

The solids distribution is illustrated by plots of slurry density in Figure 5. In both tanks, the predicted solids distribution is very uniform except for a region of lower concentration near the surface. This is consistent with the presence of a clarified layer as obtained in plant operation. However, the solids concentrations near the surface are very similar for both tanks, which does not agree with plant experience. Here, the solids concentration predicted by the model would depend upon a balance between the mean velocity of the liquor and the particle settling velocity, and concentrations are similar because the mean velocities are similar in each tank. This suggests a shortcoming in these simulations, due to the steady-state assumption and use of the RANS equations. The flow is more likely to be inherently unsteady. To gain further insight, the transient flow structures were simulated using LES.
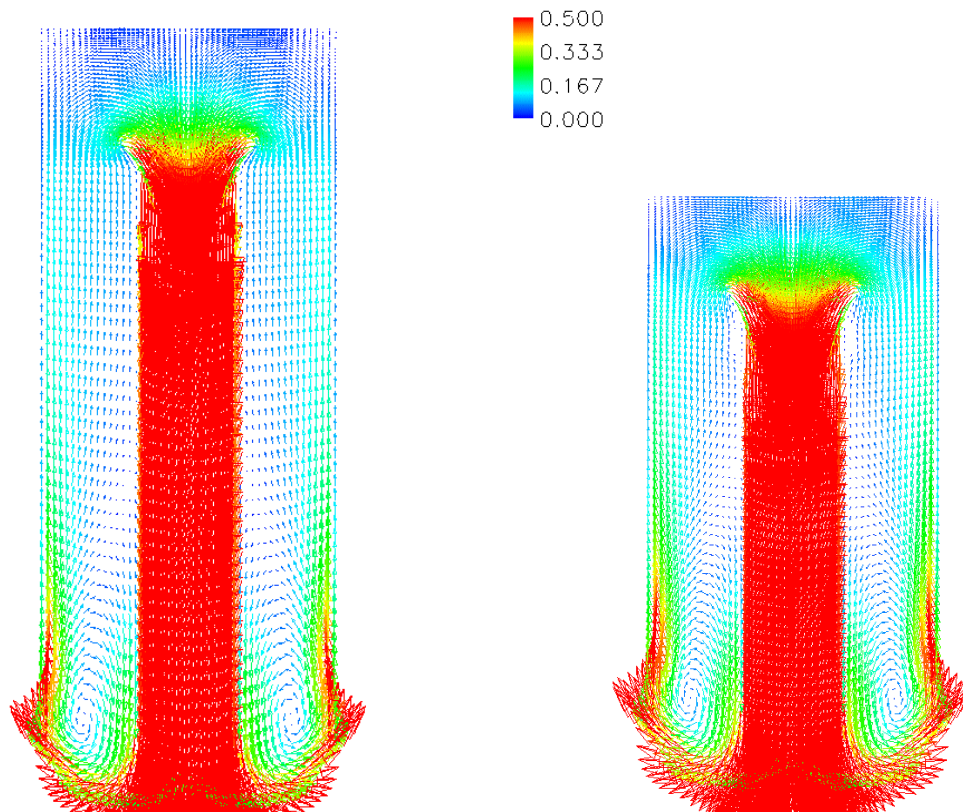

Figure 3: Comparison of mean velocity vectors (m/s) for tanks shown at same scale.

Large eddy simulations

Results obtained from the large eddy simulations are illustrated by Figures 6 – 8. These plots represent snapshots in time toward the end of the calculation. The plots are intended to illustrate typical turbulent conditions, although the instantaneous flow pattern is quite variable and the flow can be better understood from animations. Time averages have been extracted from the later part of each simulation, and a similar time-averaged flow field is recovered as was obtained in the steady-state mode, with a recirculating vortex once again present in the lower annular region. Again, the length of the recirculating toroidal vortex is the same in both tanks, however, the length obtained from LES was longer. The discrepancy would reflect the various differences in modelling methods and assumptions, but it is not possible at this stage to discern which method is more accurate in terms of the length of the vortex, due to lack of actual velocity measurements.

The large eddy simulations show that the length of the vortex is constantly changing, with constant changes in the positions of attachment or separation from the draft tube and outer walls in the upper part of the annulus, and flow reversals near the points of attachment and detachment. Associated with these variations in the vortex, there are surges of turbulence towards the surface. Since the vortex is the same length, these bursts of turbulence reach the surface of the shorter tank with greater intensity and frequency.

To assess the level of turbulence near the surface, the average turbulent kinetic energy associated with the resolved eddy structures has been calculated from the transient solution. This turbulent kinetic energy is plotted for each tank in Figure 8. Whereas the steady-state solutions suggested that the turbulent kinetic energy in the region above the draft tube was about the same for each tank, LES results indicate that the top part of the tank is considerably more turbulent for the shorter tank.

Hence, the LES results provide confirmation of what was inferred from the steady-state model, namely that the toroidal recirculating vortex is highly turbulent and unstable, with the same length in both vessels. Since the artificial constraint of a steady state condition has been removed in the LES, this method has shown more clearly the effects on flow near the surface. In the shorter tank there is considerably more frequent upward surging of the flow, and this surging would be responsible for the transport of solids into the clarifying layer.

To improve clarification of the overflow, modifications to the design of the shorter tank might be made. Such modifications might possibly include some form of baffling, so as to control the flow pattern in the annulus. Further CFD modelling might be of assistance in investigating such modifications to the design.

CONCLUSION

Investigations have been carried out for the flow in two precipitators with draft tube circulators. The precipitator tanks had the same draft tube diameter and overall diameter, but differing aspect ratios. Initial steady-state simulations revealed a region of recirculation in the lower part of the vortex. The high turbulence intensities obtained with the RANS equations suggested that the flow in this recirculating vortex could be unstable. This was confirmed by carrying out large eddy simulations. The higher solids in the overflow of the shorter tank can be explained in terms of the closer proximity of the unstable recirculating zone, so that bursts of turbulence transport solids more readily into the clarifying layer.
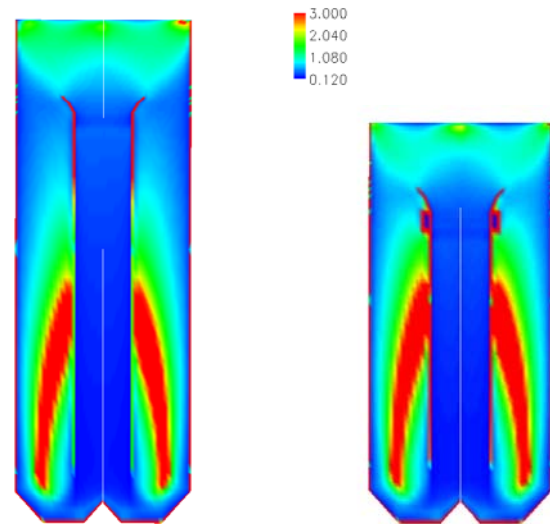

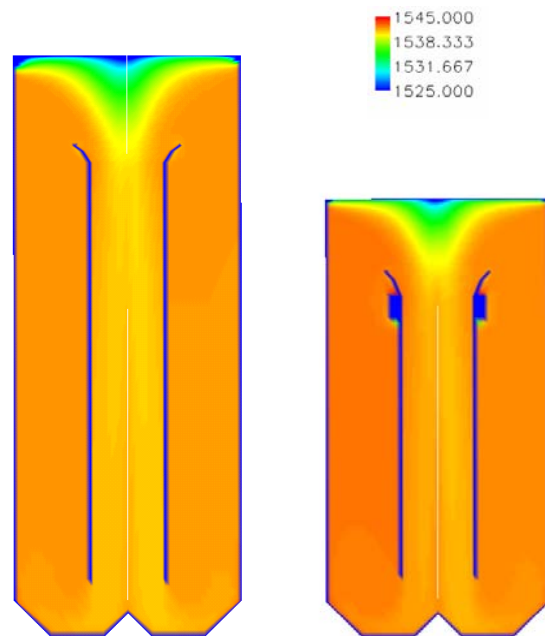**Figure 4**: Comparison of turbulence intensity in a vertical plane through tank centre.

Figure 5. Slurry density (kg/m^3) plotted in a vertical slice through tank centre.
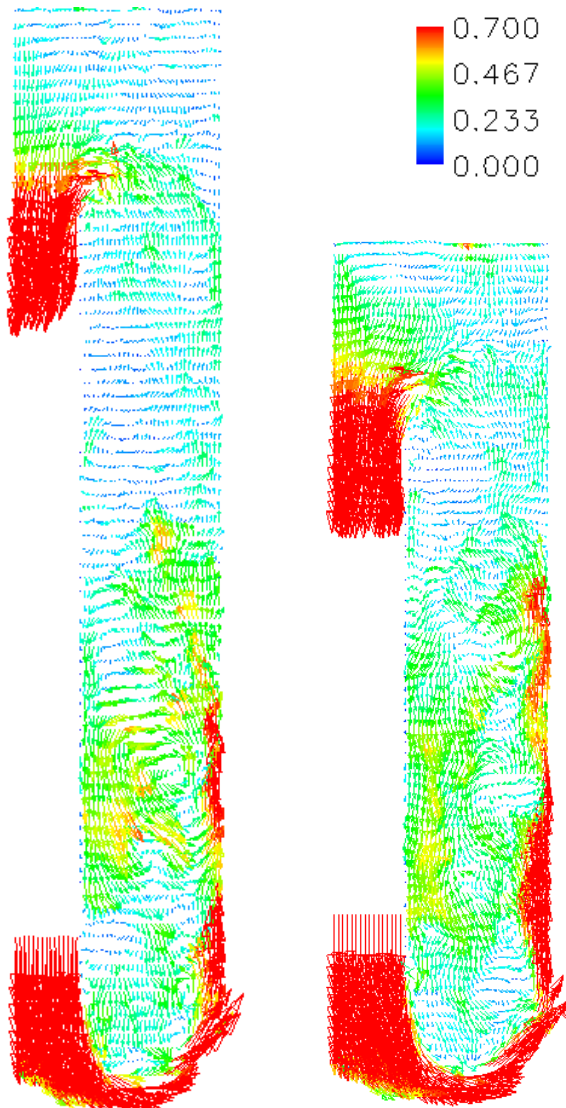
5

Figure 6. Typical snapshot of flow in taller and shorter tanks in a vertical plane using LES method. For clarity, vectors are plotted on a coarser grid than actual finite volume mesh.

REFERENCES

AESCHBACH, S. & BOURNE, J.R. (1972), "The Attainment of Homogeneous Suspension in a Continuous Stirred Tank", *Chem Eng J*, **4**, 234–242.

AUBIN, J., NAUDE, I. BERTRAND, J. & XUEREB, C. (2000), "Blending of Newtonian and shear-thinning fluids in a tank stirred with a helical screw agitator", *Trans IChemE*, **78**, Part A, 1105–1114.

EGGELS, J.G.M. (1996), "Direct and large eddy simulations of turbulent fluid flow using the lattice-Boltzmann scheme", *Int J Heat Fluid Flow*, **17**, 307–323.

HARTMANN, H., DERKSEN, J.J., MONTAVON, C., PEARSON, J., HAMILL, I.S., & VAN DEN AKKER, H.E.A. (2004), "Assessment of large eddy and RANS stirred tank simulations by means of LDA", *Chem Eng Sci*, **59**, 2419–2432.

KUMARESAN, T., NERE N.K. & JOSHI, J.B. (2005), "Effect of Internals on the Flow Pattern and Mixing in Stirred Tanks", *Ind Eng Chem Res*, 2005, **44**, 9951-9961.

PAUL, E.L., ATIEMO-OBENG, V.A. & KRESTA, S.M. (2004), *Handbook of Industrial Mixing: Science and Practice*, John Wiley & Sons, 2004.

SHAW, J.A. (1982), "The Design of Draft Tube Circulators", *Proceedings of the Australasian Institute of Mining and Metallurgy*, No. 283, 47–58.
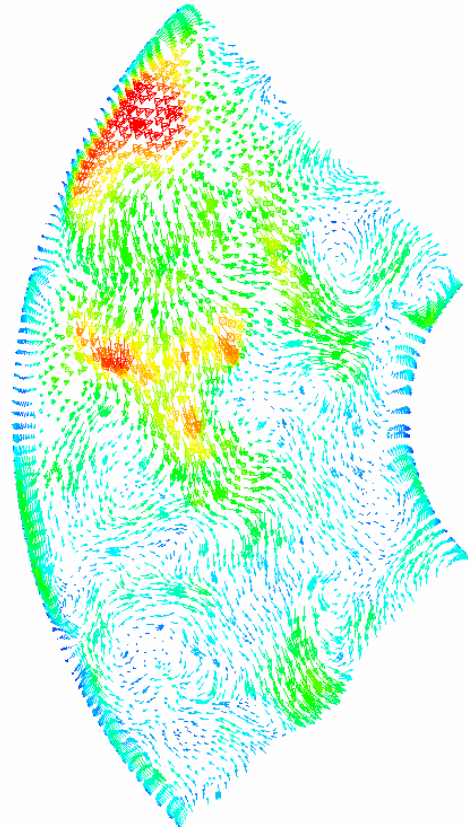
Figure 7. Snapshot of flow in a horizontal plane in the taller tank, at about the middle of the annulus, using the LES method. Actual grid resolution shown.
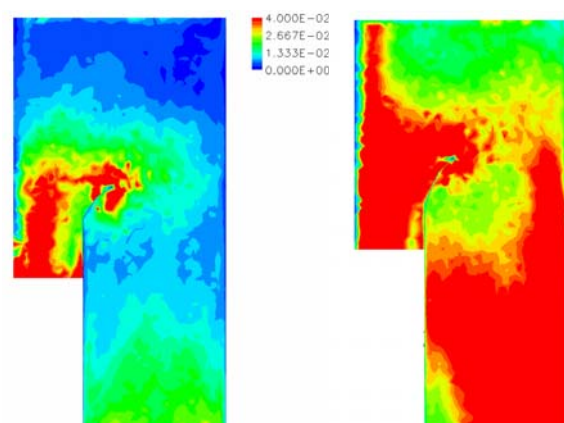

Figure 8. Turbulent kinetic energy (m^2/s^2) of the resolved portion of the turbulence near top of tank: comparison of taller and shorter tanks (on left and right respectively).